IEEE Access
Multidisciplinary ⋮ Rapid Review ⋮ Open Access Journal

Received 18 January 2024, accepted 3 March 2024, date of publication 7 March 2024, date of current version 14 March 2024.

Digital Object Identifier 10.1109/ACCESS.2024.3374378

RESEARCH ARTICLE

Compact 2 × 2 Dual-Polarized Patch Antenna Array Transmitting Eight Uncorrelated Waves for the WiFi-6E MIMO Access Point Featuring Eight Spatial Streams

KIN-LU WONG[1,2], (Fellow, IEEE), TZU-CHUN WEI[1], (Student Member, IEEE), YU-SHEN TSENG[1], (Student Member, IEEE), AND WEI-YU LI[3], (Member, IEEE)

[1]Department of Electrical Engineering, National Sun Yat-sen University, Kaohsiung 80424, Taiwan
[2]6G Communication and Sensing Research Center, National Sun Yat-sen University, Kaohsiung 80424, Taiwan
[3]Information and Communications Research Laboratories, Industrial Technology Research Institute, Hsinchu 31057, Taiwan

Corresponding author: Kin-Lu Wong (wongkl@mail.nsysu.edu.tw)

This work was supported in part by the National Science and Technology Council, Taiwan, under Grant NSTC 112-2218-E-110-004.

ABSTRACT The WiFi 6E extends the WiFi 6 operation in the 6 GHz band and features the 8 × 8 MIMO system. Recently, many countries have also made the lower 6 GHz band (5.925-6.425 GHz) available for the license-exempt wireless local area network, including the WiFi 6E. For such MIMO systems featuring 8 spatial streams in the lower 6 GHz band, we propose the compact 2 × 2 dual-polarized patch (DPP) antenna array with 8 isolated ports in a small size of 40 mm × 40 mm (about $0.66\lambda^2$ at 5.9 GHz) to transmit 8 uncorrelated waves for the WiFi-6E MIMO access point featuring 8 spatial streams. In addition, over the operating band, the isolation of any two ports thereof is larger than 20 dB and the maximum port isolation is larger than 30 dB. The high port isolation of the compact 2 × 2 DPP antenna array is owing to each DPP antenna therein clad with an L-shape metal wall. We also test the fabricated compact DPP antenna array and its application in the 8 × 8 MIMO system in an on-campus public indoor space. The measured 8 × 8 MIMO system capacity reaches about 53 bps/Hz, even though the tested public indoor space is not an ideally rich multipath environment. The obtained results imply that for the maximum 160 MHz channel in the WiFi-6E, the system capacity based on using the compact DPP antenna array in the practical public indoor space can be about 8.48 Gbps (53 bps/Hz × 160 MHz), which reaches 88% of the WiFi-6E's ideal projected system capacity of 9.6 Gbps. We present in this study the proposed compact DPP antenna array and its measured 8 × 8 MIMO system results.

INDEX TERMS MIMO antennas, compact dual-polarized patch antenna arrays, WiFi-6E MIMO access-point antennas, 8 × 8 MIMO systems, the lower 6 GHz band.

I. INTRODUCTION

The WiFi 6E named by the WiFi Alliance [1] extends the WiFi 6 in the 6 GHz band and features up to 8 × 8 multi-input-multi-output (MIMO) systems [1], [2], [3]. It is also noted that the lower 6 GHz band (5.925-6.425 GHz) has recently been made available for the license-exempt wireless local area network, including the WiFi 6E, in many countries [4], [5]. For the upcoming 8 × 8 WiFi MIMO system, the antennas in the access point thereof require to transmit 8 uncorrelated spatial streams. In order to obtain high signal-to-noise ratio (SNR) received by the terminal device at the receiver side and rich multipath scattering in the MIMO environment between the receiver and transmitter, the multiport (3-port [6], [7], [8], [9], [10], 4-port [11], [12], [13], [14], [15], [16], or 6-port [17], [18]) patch antennas have been reported for the MIMO access-point application.

The associate editor coordinating the review of this manuscript and approving it for publication was Luyu Zhao.

Such multiport patch antennas [6], [7], [8], [9], [10], [11], [12], [13], [14], [15], [16], [17], [18] are characterized by their compact antenna size with a back ground plane to transmit multiple (3, 4, or 6) uncorrelated waves mainly in the antenna's front hemisphere. The transmitted waves can therefore have enhanced antenna gain as compared to the monopole-type antennas with bi-directional radiation [19]. This can lead to increased SNR for receive (Rx) antennas of the terminal device in the MIMO system. In addition, the waves transmitted by such patch antennas still have a wide beamwidth as the monopole-type antennas in the front half-space to provide rich multipath signals in the environment of the MIMO system.

Two 4-port patch antennas in a 1 × 2 array to provide 8 transmit antennas in the MIMO system featuring 8 spatial streams have also been reported [20], [21], [22]. For the 8 × 8 MIMO system, the measured system capacity can reach about 42 bps/Hz [20]. However, in order to achieve good isolation of two ports in different 4-port patch antennas, the simple way of placing a large spacing (about one wavelength) between the two 4-port patch antennas is used. This greatly increases the total size of the multiport patch antenna array to provide 8 transmit antennas for the 8 × 8 MIMO system.

Another way is the use of 8 planar monopoles arranged in a circular array and backed by a large ground plane to transmit 8 uncorrelated waves mainly in the antenna's front half-space [23], similar to the patch antenna. The measured 8 × 8 MIMO system capacity is also similar to that in [20]. However, the 8 planar monopoles have a high profile of larger than 0.2 wavelength above the ground plane [23].

On the other hand, it is known that the patch antenna generally has a relatively much lower profile. Recently, it is reported to generate 8 uncorrelated waves by using a 2 × 2 dual-polarized patch (DPP) antenna array [24], which is promising to be applied in the 8 × 8 MIMO system. The 2 × 2 antenna array is formed by four DPP antennas [25], [26] with each one generating 2 dual-polarized waves. The 2 × 2 antenna array is operated in the 2.4-2.5 GHz, suitable for the WiFi MIMO system.

It is noted that its antenna substrate has an effective relative permittivity of about 2.3, which reduces the array size to be about $1.39\lambda_g^2$ with respect to the guided wavelength (λ_g) and the lower-edge frequency (2.4 GHz) of the operating band. The equivalent array size per wave is therefore about $0.17\lambda_g^2$ only. However, for the 2 × 2 antenna array with a compact size to achieve enhanced port isolation, an external large decoupling network of size about $4.8\lambda_g^2$ is introduced. The maximum port isolation is larger than 30 dB and the minimum port isolation over the operating band is about 15 dB [24].

Recently, the 2 × 2 patch antenna array is also reported to generate two dual-polarized waves over a wide band of about 5.1-7.5 GHz for the WiFi application [27]. This interesting 2 × 2 array, however, has only 2 ports. The 2 × 2 array generates only 2 dual-polarized waves and is not suitable to be applied in the 8 × 8 MIMO system. In this case, the equivalent array size per wave is about $0.25\lambda_g^2$, which is much larger than that for the 2 × 2 DPP antenna array in [24].

In this study, we propose a compact 2 × 2 DPP antenna array with 8 isolated ports in a small size of 40 mm × 40 mm to transmit 8 uncorrelated waves for the WiFi-6E 8 × 8 MIMO access point covering the lower 6 GHz band (5.925-6.425 GHz). The compact antenna array consists of 4 DPP antennas printed on a thin (0.4 mm) FR4 substrate and mounted 4.6 mm above a ground plane. That is, the array height is 5 mm only and the effective relative permittivity of the array substrate is about 1.07, close to unity. The array height is therefore about $0.1\lambda_g^2$, much less than that of the 8-planar monopole array in [23].

The array size is also about $0.66\lambda_g^2$ only, with an equivalent array size per wave about $0.083\lambda_g^2$, which is much smaller than $0.17\lambda_g^2$ for the 8-port 2 × 2 array (four DPP antennas) in [24] and $0.18\lambda_g^2$ for the 8-port 1 × 2 array (two 4-port patch antennas) in [20], [21], and [22]. In addition, for the proposed compact antenna array to provide 8 transmit antennas, the port isolation of any two ports thereof is larger than 20 dB over the operating band, with the maximum port isolation larger than 30 dB therein.

The enhanced port isolation of the proposed compact DPP antenna array is achieved by using four DPP antennas clad with an L-shape metal wall. In this case, without any additional decoupling network used in [24] or decoupling element needed, enhanced port isolation is obtained in the proposed compact 8-wave MIMO antenna array to generate 8 uncorrelated waves. This is mainly because the metal wall-clad DPP antennas decrease the fringing fields around the antenna's patch edges, thus allowing the use of a smaller edge-to-edge spacing (about $0.22\lambda_g$) between adjacent antennas in the proposed 8-port 2 × 2 array.

A comparison of the proposed compact 8-port 2 × 2 DPP antenna array (this work) with the above mentioned patch antenna arrays to transmit 8 uncorrelated waves [20], [21], [22], [24] for the 8 × 8 MIMO access-point application is also listed in Table 1. The proposed design presents a compact 8-wave MIMO antenna array promising for the WiFi-6E 8 × 8 MIMO access-point application in the lower 6 GHz band. Details of the proposed design are presented. The design considerations of the 4 DPP antennas clad with an L-shape metal wall for enhanced port isolation are addressed.

The fabricated 2 × 2 DPP antenna array is experimentally studied and also tested in an 8 × 8 MIMO system in a practical public indoor space in the campus of the National Sun Yat-sen University (NSYSU). It is worthy to note that the obtained 8 × 8 MIMO system capacity reaches about 53 bps/Hz, although the tested public indoor space in this study is not an ideally rich multipath environment for the 8 × 8 MIMO system. The obtained results imply that for the maximum 160 MHz channel in the WiFi 6E [2], the system capacity in our tested on-campus public indoor space can be about 8.48 Gbps (53 bps/Hz × 160 MHz), reaching about 88% of the WiFi-6E's ideal projected system capacity of

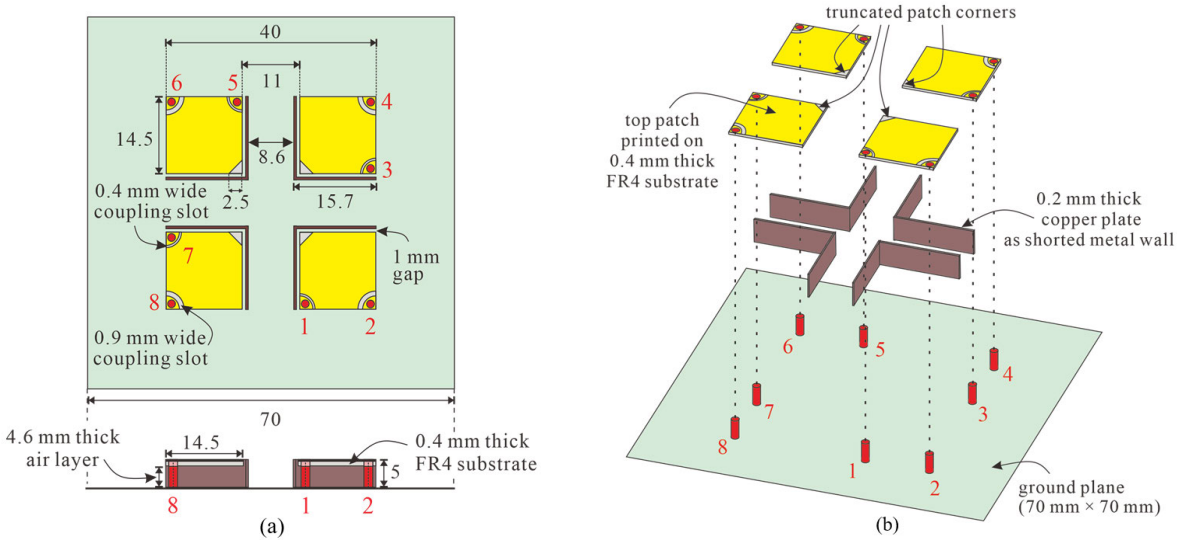

FIGURE 1. Geometry of the compact 2 × 2 DPP antenna array with Ports 1-8 transmitting 8 uncorrelated waves for the WiFi-6E MIMO access point featuring 8 spatial streams. (a) Top and side views. (b) Exploded view.

TABLE 1. Compariso n of the proposed compact 2 × 2 DPP antenna array (this work) with the patch antenna arrays to transmit 8 uncorrelated waves [20], [21], [22], [24] for the 8 × 8 MIMO access-point application.

[Ref]	[20], [21], [22]	[24]	This work
Total ports in the antenna array	8 ports (1 X 2 array)	8 ports (2 X 2 array)	8 ports (2 X 2 array)
Transmitting 8 uncorrelated waves	Yes (two 4-port patch antennas for 8 waves)	Yes (four DPP antennas for 8 waves)	Yes (four DPP antennas for 8 waves)
Operating band	5.9-8.5 GHz	2.4-2.5 GHz	5.9-6.5 GHz
Array substrate's relative permittivity	close to 1, about 1.07	about 2.3	close to 1, about 1.07
Array height in guided wavelength (λ_g)	5.0 mm ($0.10\lambda_g$@5.9GHz)	4.762 mm ($0.058\lambda_g$@2.4GHz)	5.0 mm ($0.10\lambda_g$@5.9GHz)
Array size in guided wavelength (λ_g)	31 X 111 mm^2 ($1.42\lambda_g^2$@5.9GHz)	97.2 X 97.2 mm^2 ($1.39\lambda_g^2$@2.4GHz)	40 X 40 mm^2 ($0.66\lambda_g^2$@5.9GHz)
Equivalent array size per wave	$0.18\lambda_g^2$@5.9GHz	$0.17\lambda_g^2$@2.4GHz	$0.083\lambda_g^2$@5.9GHz
Patch edge-to-edge spacing	49 mm ($0.99\lambda_g$@5.9GHz)	25.2 mm ($0.30\lambda_g$@2.4GHz)	11 mm ($0.22\lambda_g$@5.9GHz)
Minimum port isolation in operating band	20 dB (max. isolation > 30 dB)	15 dB (max. isolation > 30 dB)	20 dB (max. isolation > 30 dB)
External decoupling network	No	Yes (size 180 X 180 mm^2, $4.8\lambda_g^2$@2.4GHz)	No

9.6 Gbps [3]. This indicates that the proposed compact DPP antenna array is promising for the WiFi-6E application; and furthermore, its ideal projected system capacity of 9.6 Gbps is very likely to be feasible for the 8 × 8 MIMO system operated in the practical indoor environment.

In the following sections, we introduce the compact 2 × 2 DPP antenna array in Section II and address the design considerations and parametric study, respectively, in Sections III and IV. We also study the fabricated compact DPP antenna array in Section V and apply it in the 8 × 8 MIMO system tested in a practical on-campus public indoor space in Section VI. Finally, we summarize the conclusion in Section VII.

II. THE COMPACT 2 × 2 DPP ANTENNA ARRAY

Fig. 1 shows the proposed compact 2 × 2 DPP antenna array with Ports 1-8 transmitting 8 uncorrelated waves for the WiFi-6E 8 × 8 MIMO access-point application.

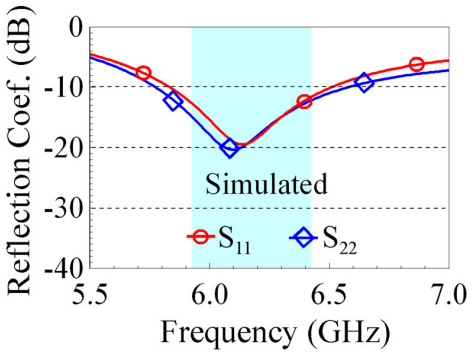

FIGURE 2. Simulated reflection coefficients of Ports 1 and 2 in the DPP antenna array.

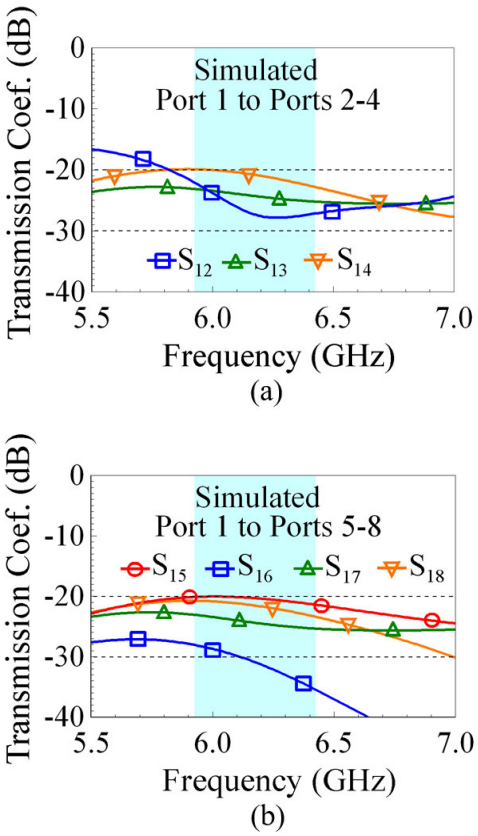

FIGURE 3. Simulated transmission coefficients of Port 1 to Ports 2-8 in the DPP antenna array. (a) The S_{12}, S_{13}, and $_{14}$. (b) The S_{15}, S_{16}, S_{17}, and S_{18}.

The 2 × 2 antenna array operates in about 5.9-6.5 GHz and covers the lower 6 GHz band (5.925-6.425 GHz). The top and side views of the antenna array are shown in Fig. 1(a); and the exploded view is shown in Fig. 1(b).

Each DPP antenna has a square top patch of size 14.5 mm × 14.5 mm printed on a 0.4 mm thick FR4 substrate (relative permittivity 4.4, loss tangent 0.02) which is mounted 4.6 mm above a ground plane of 70 mm × 70 mm. The antenna substrate thus consists of two layers (0.4 mm thick FR4 layer and 4.6 mm thick air layer) and has a thickness of 5.0 mm with an effective relative permittivity of 1.07, close to unity. In this case, the antenna height is about $0.1\lambda_g$ and the top patch size is about $0.29\lambda_g \times 0.29\lambda_g$ with respect to the guided wavelength of the antenna substrate at 5.9 GHz.

In addition, each DPP antenna is closely clad with an L-shape metal wall [gap 1 mm as shown in Fig. 1(a)], which is shorted to the ground plane along the top patch's two inner edges. The metal wall uses a 0.2 mm thick copper plate in the study. The metal wall is flush with the top patch's two outer edges and has a same height (5.0 mm) as the top patch above the ground plane. For each DPP antenna, the metal wall can suppress the fringing fields of two orthogonal half-wavelength resonant modes excited by the antenna's two probe feeds placed at two adjacent patch corners along one outer patch edge.

Owing to the decoupling metal wall, we can apply a small distance of 8.6 mm (about $0.17\lambda_g$ at 5.9 GHz) between two metal wall-clad DPP antennas. The 2 × 2 DPP antenna array therefore has a compact size of 40 mm × 40 mm ($0.81\lambda_g \times 0.81\lambda_g$ or $0.66\lambda_g^2$ at 5.9 GHz). Note that the four metal wall-clad DPP antennas are sequentially rotated by 90 degrees in the 2 × 2 array. The equivalent array size for one transmitted wave is only about $0.083\lambda_g^2$ at 5.9 GHz. With a compact array size, the port isolation between any two ports in the array is larger than 20 dB over the operating band.

Note that by placing the two probe feeds at two adjacent patch corners for each DPP antenna, the distance between the two probe feeds is maximized so that two SMA connectors on the back side of the ground plane can be applied to excite the antenna in the experimental study. In addition, in order to achieve good impedance matching for the probe feed having a length of about 0.1 wavelength, each probe feed is capacitively coupled to the top patch through a coupling quarter-ring slot.

It is also noted that, owing to adding the decoupling metal wall to suppress the fringing fields of the excited half-wavelength resonant mode, the impedance matching of the two ports in each DPP antenna undergoes different effects. By using different coupling quarter-ring slots of widths 0.4 mm and 0.9 mm for the two probe feeds, their corresponding half-wavelength resonant modes can be excited to occur at close frequencies.

Finally, by further truncating the top patch's innermost corner (a side length of 2.5 mm as seen in Fig. 1), the two half-wavelength resonant modes excited by each DPP antenna can occur at about same frequencies.

Fig. 2 shows the simulated reflection coefficients of Ports 1 and 2 in the DPP antenna array. The simulated results are obtained using the 3D High Frequency Electromagnetic Simulation Software, ANSYS HFSS version 19.1 [28].

Note that, based on using different widths of the quarter-ring slots, the S_{11} and S_{22} in Fig. 2 show similar results and are both less than -10 dB over 5.9-6.5 GHz. That is, the operating band covers the target lower 6 GHz band (5.925-6.425 GHz,

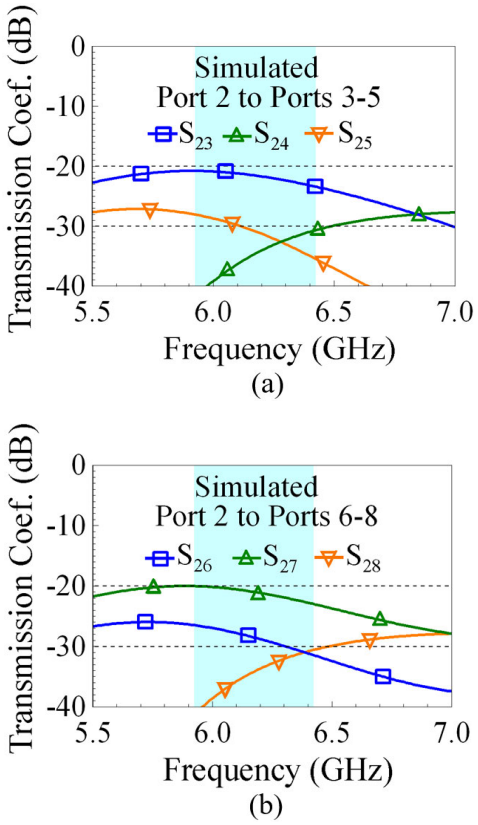

FIGURE 4. Simulated transmission coefficients of Port 2 to Ports 3-8 in the DPP antenna array. (a) The S_{23}, S_{24}, and S_{25}. (b) The S_{26}, S_{27}, and S_{28}.

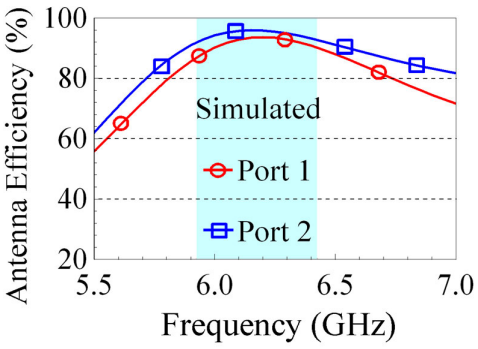

FIGURE 5. Simulated antenna efficiency of Ports 1 and 2.

see the colored frequency region in the figure). Also note that, owing the symmetric structure of the four DPP antennas in the array, Ports 3, 5, and 7 have same results as Port 1. Similarly, Ports 4, 6, and 8 have same results as Port 2.

The simulated transmission coefficients of Port 1 to Ports 2-8 in the DPP antenna array are shown in Fig. 3. The transmission coefficients for the two ports with parallel polarizations (such as the S_{14}, S_{15}, and S_{18}) and those for the two ports with orthogonal polarizations (the S_{12}, S_{13}, S_{16}, and S_{17}) are all less than -20 dB over the operating band.

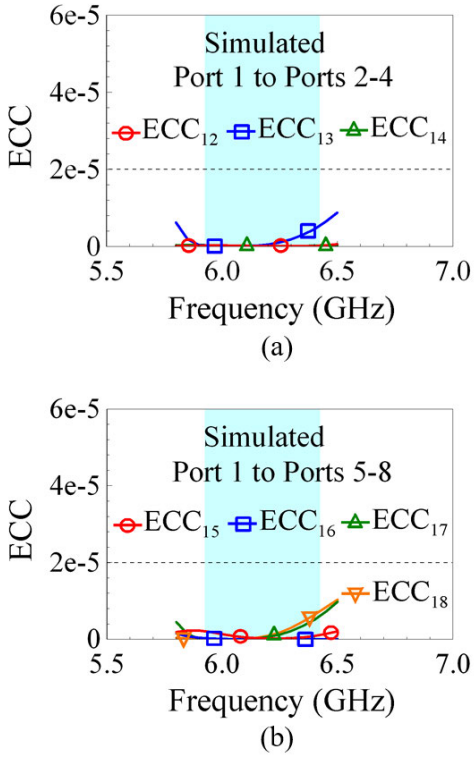

FIGURE 6. Simulated envelope correlation coefficients (ECC) of Port 1 to Ports 2-8. (a) The ECC_{12}, ECC_{13}, and ECC_{14}. (b) The ECC_{15}, ECC_{16}, ECC_{17}, and ECC_{18}.

Fig. 4 shows the simulated transmission coefficients of Port 2 to Ports 3-8 in the DPP antenna array. Similarly, the transmission coefficients for the two ports with parallel polarizations (the S_{23}, S_{26}, and S_{27}) and orthogonal polarizations (the S_{24}, S_{25}, and S_{28}) are also less than -20 dB over the operating band. The results indicate that the port isolation is larger than 20 dB for any two ports in the compact 2 × 2 DPP antenna array.

Fig. 5 shows the simulated antenna efficiency of Ports 1 and 2. The antenna efficiency includes the mismatching loss and is larger than 86% over the operating band. Note that Port 2 has an even larger antenna efficiency than Port 1. This is largely because Port 2 is located at the array corner and is not in close proximity to the metal wall, thus having relatively larger radiation efficiency than Port 1. Again, owing the symmetric array structure, Ports 4, 6, and 8 have same results as Port 2; and Ports 3, 5, and 7 have same results as Port 1.

The simulated envelope correlation coefficients (ECC) of Port 1 to Ports 2-8 are presented in Fig. 6; and the corresponding results of Port 2 to Ports 3-8 are shown in Fig. 7. The ECC_{mn} in the figure indicates the ECC of two waves excited by Ports m and n. Over the operating band, the ECC values are all less than 10^{-5}. The very small values suggest that any two waves generated by the compact DPP antenna array can be treated as uncorrelated.

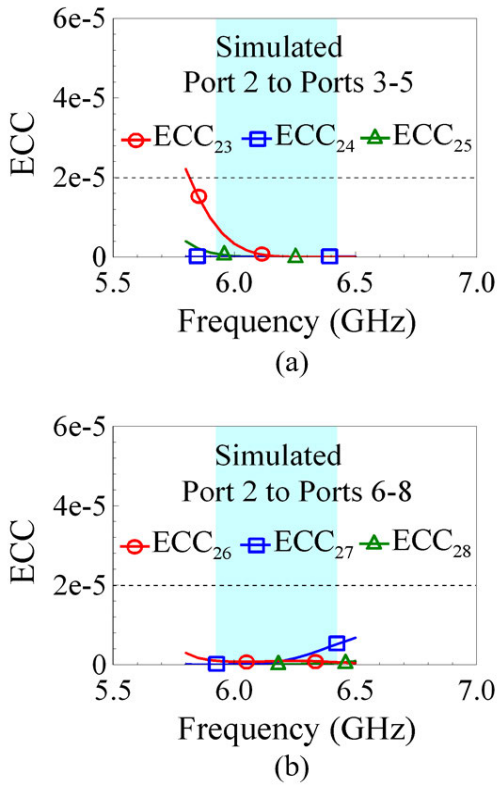

FIGURE 7. Simulated ECCs of Port 2 to Ports 3-8. (a) The ECC_{23}, ECC_{24}, and ECC_{25}. (b) The ECC_{26}, ECC_{27}, and ECC_{28}.

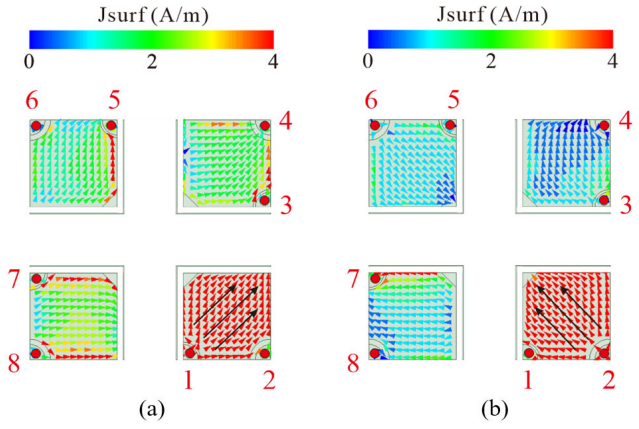

FIGURE 8. Simulated surface current distributions excited in the top patch of the DPP antenna array; $f = 6.18$ GHz. (a) Port 1 excitation. (b) Port 2 excitation.

The excited resonant modes are also analyzed. Fig. 8 shows the simulated surface current distributions in the top patch excited by Ports 1 and 2 at 6.18 GHz. For either Port 1 or Port 2 excitation, the remaining ports are terminated to 50 ohms. It is observed that the excited resonant mode is mainly resonated along the diagonal line facing the excited port.

From the simulated electric field distributions excited in the median plane (2.5 mm above the ground plane) between the top patch and ground plane shown in Fig. 9, it is also observed that there is a null electric field along the diagonal line orthogonal to the resonant direction of the excited mode.

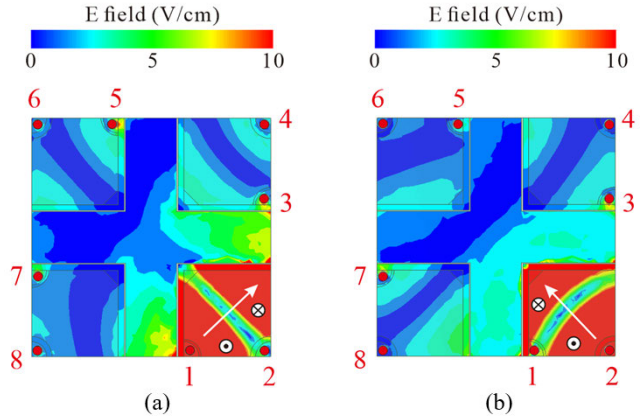

FIGURE 9. Simulated electric field distributions excited in the median plane (2.5 mm above the ground plane) between the top patch and ground plane of the DPP antenna array; $f = 6.18$ GHz.

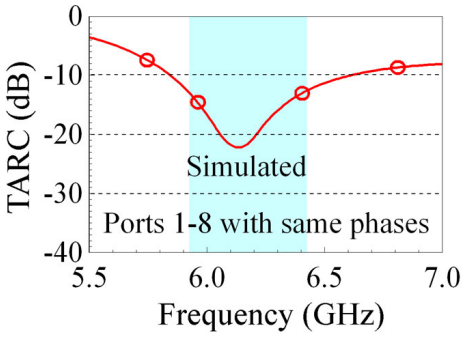

FIGURE 10. Simulated total active reflection coefficient (TARC) of the DPP antenna array; Ports 1-8 are excited with same phases.

In addition, the electric fields on two sides of the null field are in opposite phases. This characteristic indicates that either Port 1 or Port 2 excites a half-wavelength resonant mode resonated along the top patch's diagonal line. This confirms that each two-port antenna in the 2 × 2 array is a dual-polarized patch antenna.

To consider the 2 × 2 array as a whole, the simulated total active reflection coefficient (TARC) [16], [18], [29] for all Ports 1-8 excited in the array is shown in Fig. 10. The TARC value obtained for Ports 1-8 with same excitation phases is also less than −10 dB over the operating band. This may also attribute to all the port isolation in the 2 × 2 array being larger than 20 dB as seen in Figs. 3 and 4.

III. DESIGN CONSIDERATIONS

The design considerations of the 2 × 2 DPP antenna array are also addressed. Fig. 11(a) shows the geometry of the antenna array with no inner truncated patch corner and no decoupling metal wall clad for each antenna (denoted as Design A in the study). The case of Design A with the decoupling metal walls is shown in Fig. 11(b) and denoted as Design B. The case

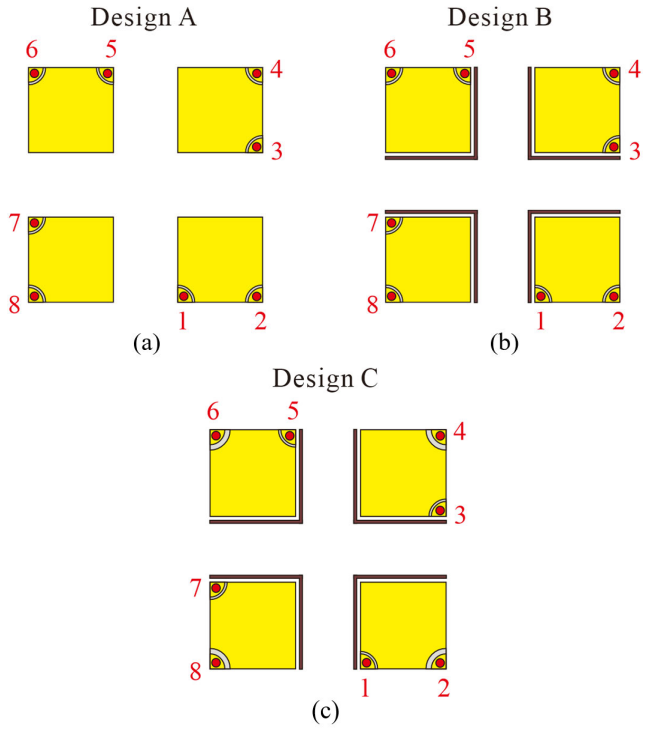

FIGURE 11. Geometries of (a) the DPP antenna array with no inner truncated patch corner and no decoupling metal wall clad for each antenna (denoted as Design A), (b) the case of Design A with decoupling metal walls (denoted as Design B), and (c) the case of Design B with a larger coupling slot width (0.9 mm) for Ports 2, 4, 6, 8 than that (0.4 mm) for Ports 1, 3, 5, 7 (denoted as Design C).

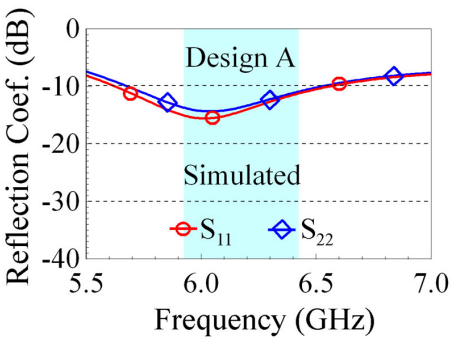

FIGURE 12. Simulated reflection coefficients of Ports 1 and 2 in Design A.

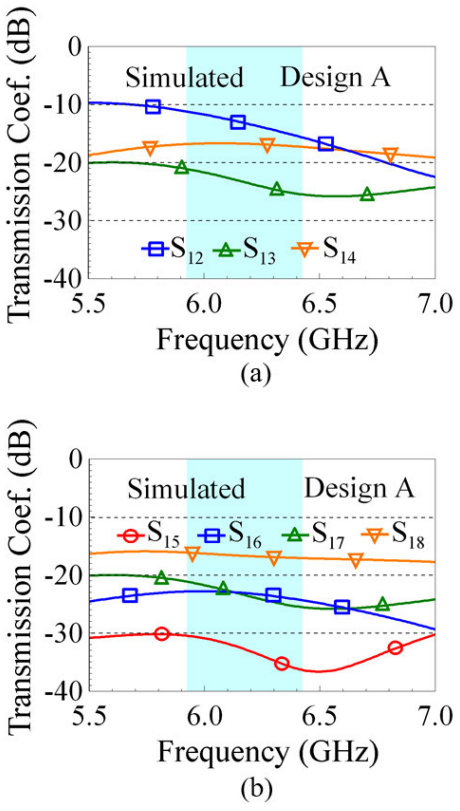

FIGURE 13. Simulated transmission coefficients of Port 1 to Ports 2-8 in Design A. (a) The S_{12}, S_{13}, and S_{14}. (b) The S_{15}, S_{16}, S_{17}, and S_{18}.

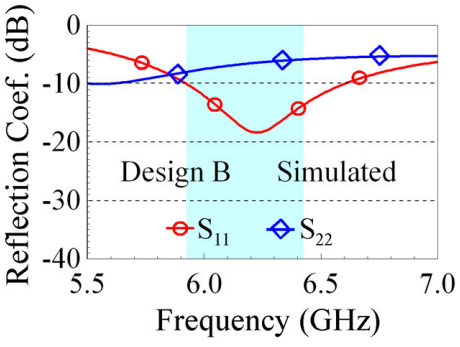

FIGURE 14. Simulated reflection coefficients of Ports 1 and 2 in Design B.

of Design B with a larger coupling slot width (0.9 mm) for Ports 2, 4, 6, 8 than that (0.4 mm) for Ports 1, 3, 5, 7 is shown in Fig. 11(c) and denoted as Design C.

Note that the coupling slot widths for Ports 1-8 in Design A and B are all fixed as 0.4 mm. The proposed design in Fig. 1 is finally obtained by truncating the four top patch's innermost corners in Design C. The corresponding dimensions in Design A, B, and C are same as those shown in Fig. 1.

Fig. 12 shows the simulated reflection coefficients of Ports 1 and 2 in Design A. The S_{11} and S_{22} are less than -10 dB over the lower 6 GHz band. However, the simulated transmission coefficients of Port 1 to Ports 2-8 in Design A [see Fig. 13(a) and (b)] cannot all be less than −20 dB.

For instance, in Design A, the S_{14} and S_{18} of two ports in adjacent DPP antennas with parallel polarizations are respectively less than −17 dB and -16 dB only. The S_{12} of two ports in each DPP antenna is even less than −12 dB only. This behavior is largely owing to the coupling effects caused by the four DPP antennas being closely arranged to form the proposed compact array.

Fig. 14 shows the simulated reflection coefficients of Ports 1 and 2 in Design B; and the corresponding simulated

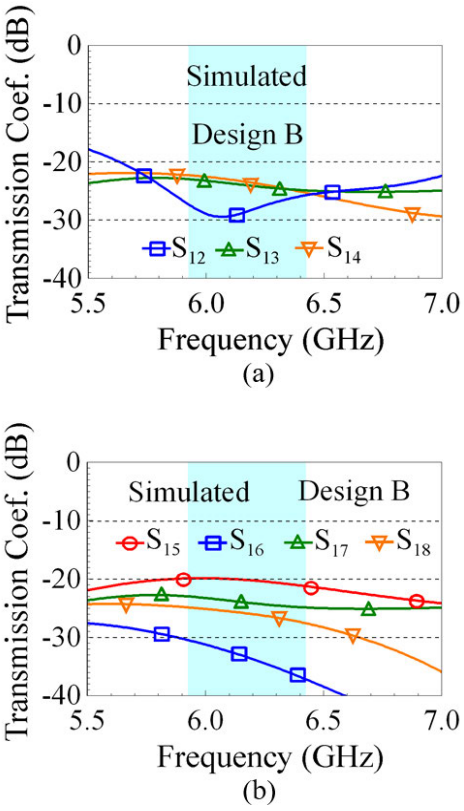

FIGURE 15. Simulated transmission coefficients of Port 1 to Ports 2-8 in Design B. (a) The S_{12}, S_{13}, and S_{14}. (b) The S_{15}, S_{16}, S_{17}, and S_{18}.

transmission coefficients of Port 1 to Ports 2-8 are presented in Fig. 15.

Due to adding the metal wall clad to each DPP antenna, the transmission coefficients of any two ports in Design B are less than −20 dB over the operating band. However, the S_{22} of Port 2 is greatly degraded; and the S_{11} of Port 1 is still less than −10 dB over the operating band. The different effects on the impedance matching of Ports 1 and 2 are mainly because the decoupling metal wall appears to be asymmetric with respect to the resonant modes excited by the two ports.

To fix the degraded S_{22} of Port 2, we adjust the coupling slot width for Port 2 (those for Ports 4, 6, and 8 also adjusted accordingly) to be 0.9 mm in Design C. Fig. 16 shows the simulated reflection coefficients of Ports 1 and 2 in Design C; and the corresponding simulated transmission coefficients of Port 1 to Ports 2-8 are presented in Fig. 17. The results show that the S_{22} in Design C is improved to be less than -10 dB over the lower 6 GHz band. In this case, the transmission coefficients of any two ports remain to be less than -20 dB.

In order to further adjust both S_{11} and S_{22} of Ports 1 and 2 to have more similar impedance matching over the operating band, the four top patch's innermost corners are truncated as seen in Fig. 1. The innermost patch corner truncation can adjust the resonant length of the resonant mode excited by Port 2, with the resonant mode excited by Port 1 relatively slightly varied. In this case, the obtained S parameters as

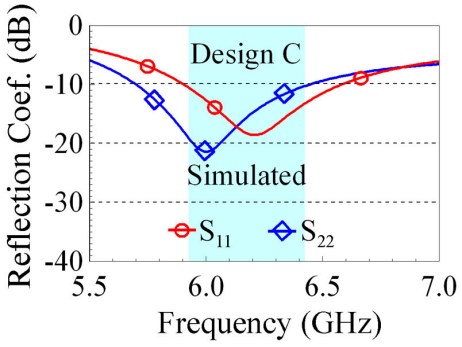

FIGURE 16. Simulated reflection coefficients of Ports 1 and 2 in Design C.

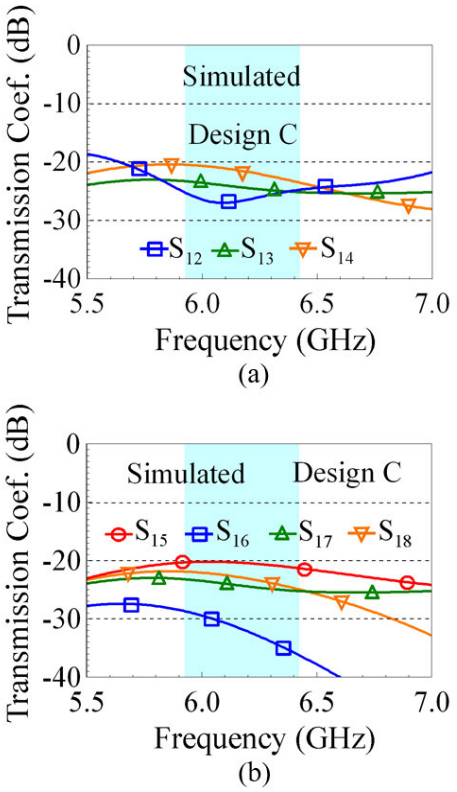

FIGURE 17. Simulated transmission coefficients of Port 1 to Ports 2-8 in Design C. (a) The S_{12}, S_{13}, and S_{14}. (b) The S_{15}, S_{16}, S_{17}, and S_{18}.

shown in Figs. 2, 3, and 4 are obtained for the proposed compact antenna array.

IV. PARAMETRIC STUDY

Typical parameters such as the gap between the metal wall and top patch for each DPP antenna, the height of the metal wall, and the distance between adjacent metal wall-clad DPP antennas are also studied. Fig. 18(a)-(d) show the simulated S parameters for varying the gap (g) between the metal wall and top patch from 0.8 mm to 1.2 mm.

The results of the reflection coefficients S_{11} and S_{22} for Ports 1 and 2 and the transmission coefficients for Port 1 to Ports 2-8 are shown. It appears that the effect on the S_{22} is

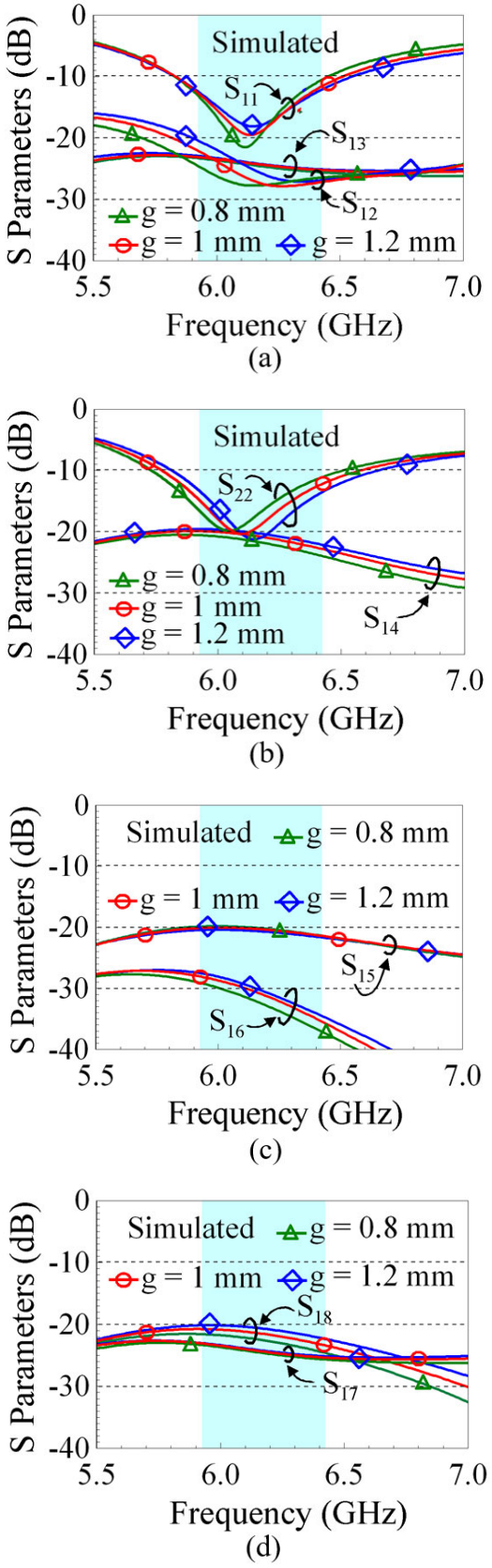

FIGURE 18. Simulated S parameters for varying the gap (g) between the metal wall and top patch from 0.8 mm to 1.2 mm. (a) The S_{11}, S_{12}, S_{13}. (b) The S_{22}, S_{14}. (c) The S_{15}, S_{16}. (d) The S_{17}, S_{18}.

relatively larger than on the S_{11}. This effect is reasonable, because the L-shape metal wall mainly faces the resonant direction of the half-wavelength resonant mode excited by Port 2.

Relatively stronger effects on the S_{12} [See Fig. 18(a)], the S_{14} [see Fig. 18(b)], and the S_{18} [see Fig. 18(d)] are also seen. When a smaller gap (for example, 0.8 mm) is selected, the transmission coefficients such as the S_{12}, S_{14}, and S_{18} can be decreased; however, the impedance matching (the S_{22}) of Port 2 is relatively strongly affected. To achieve good impedance matching of Ports 1 and 2 over the target lower 6 GHz band and also at least 20 dB port isolation of Ports 1-8, the gap g is chosen to be 1 mm in the proposed design.

Fig. 19(a)-(d) show the simulated S parameters for varying the height (h) of the metal walls from 4 mm to 6 mm. When the h is selected to be 6 mm (that is, the metal wall is higher than the top patch which is 5 mm above the ground plane), the S_{11} is quickly degraded [See Fig. 19(a)]. The S_{22} is also seen to be greatly varied [See Fig. 19(b)].

On the other hand, when the h is lower (for example, 4 mm), the S_{12} [See Fig. 19(a)], the S_{14} [See Fig. 19(b)], and the S_{18} [See Fig. 19(d)] are also increased to be larger than -20 dB. That is, all the port isolation in the compact antenna array cannot be larger than 20 dB. The height of the metal walls in this study is thus chosen to be 5 mm, same as that of the four DPP antennas.

Fig. 20(a)-(d) show the simulated S parameters for varying the distance (d) between adjacent metal walls from 6.6 mm to 10.6 mm. Note that a smaller d can make the compact antenna array with an even smaller size. When the d is smaller (for example, 6.6 mm which is 2 mm less than the chosen distance 8.6 mm in this study), the impedance matching [the S_{11}, S_{22} in Fig. 20(a) and (b)] of Ports 1 and 2 is not strongly affected. However, the S_{14} [See Fig. 20(b)], the S_{15} [See Fig. 20(c)], and the S_{18} [See Fig. 20(d)] become larger than -20 dB. To achieve larger than 20 dB port isolation for any two ports in the compact antenna array, the distance d is chosen to be 8.6 mm as seen in Fig. 1.

V. FABRICATED 2 × 2 DPP ANTENNA ARRAY

The proposed 2 × 2 DPP antenna array is fabricated for the experimental study. Fig. 21 shows the fabricated DPP antenna array. Fig. 22 shows the measured reflection coefficients of Ports 1-8 in the fabricated array. Note that in Fig. 22(a), Ports 1, 3, 5, and 7 are with same symmetric locations in the array; and in Fig. 22(b), Ports 2, 4, 6, and 8 are located at the four corners of the array and also with symmetric locations.

The corresponding transmission coefficients of Port 1 to Ports 2-4 and Ports 5-8 are respectively shown in Fig. 23(a) and (b). Those for Port 2 to Ports 3-5 and Ports 6-8 are respectively shown in Fig. 24(a) and (b). The measured reflection coefficients are less than -10 dB in the target lower 6 GHz band of 5.925-6.425 GHz and generally confirm the simulated results. The transmission coefficients also generally

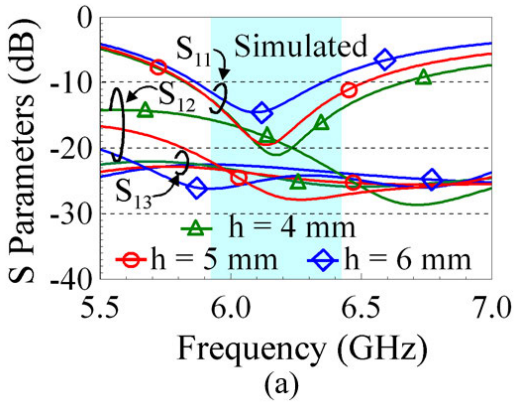

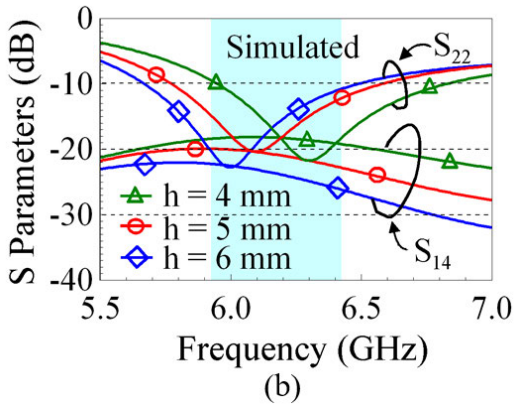

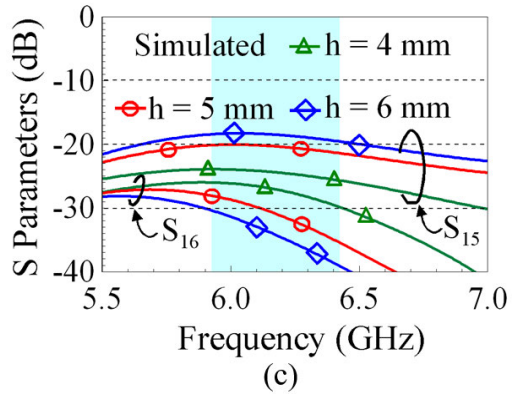

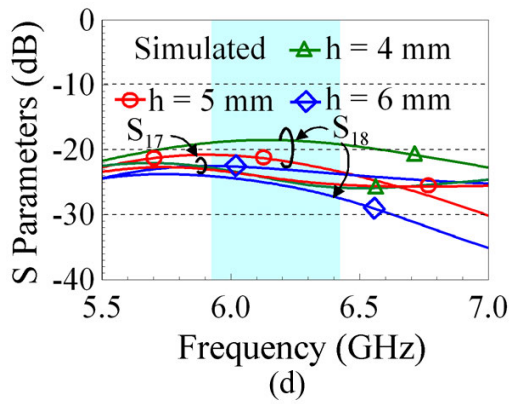

FIGURE 19. Simulated S parameters for varying the height (h) of the metal walls from 4 mm to 6 mm. (a) The S_{11}, S_{12}, S_{13}. (b) The S_{22}, S_{14}. (c) The S_{15}, S_{16}. (d) The S_{17}, S_{18}.

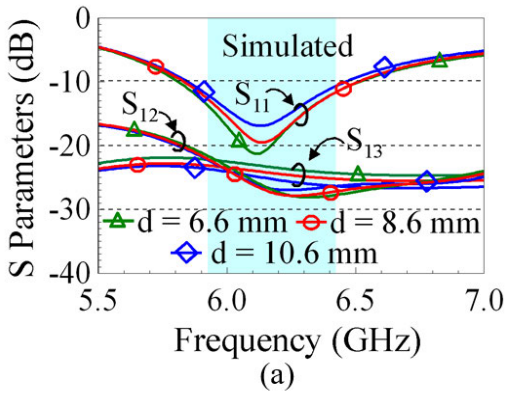

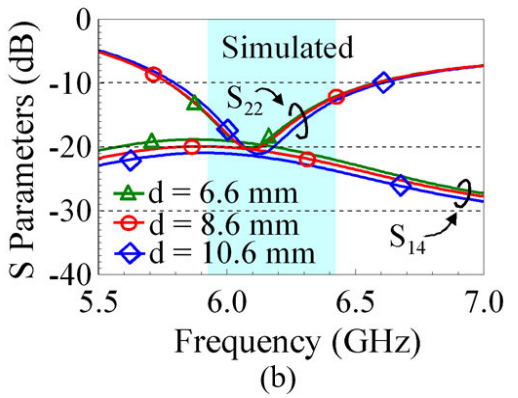

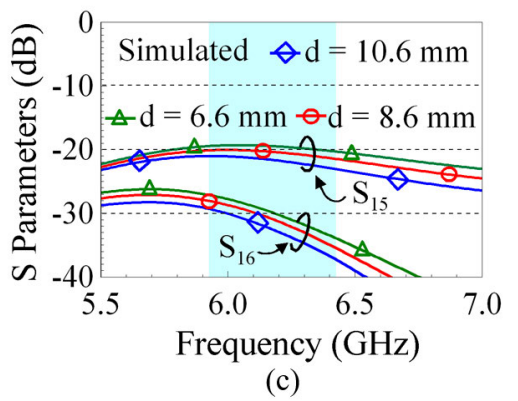

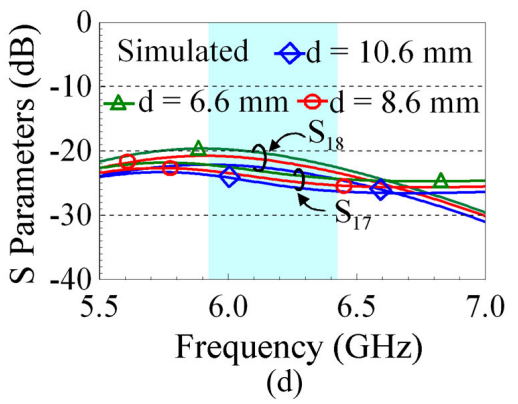

FIGURE 20. Simulated S parameters for varying the distance (d) between adjacent metal walls from 6.6 mm to 10.6 mm. (a) The S_{11}, S_{12}, S_{13}. (b) The S_{22}, S_{14}. (c) The S_{15}, S_{16}. (d) The S_{17}, S_{18}.

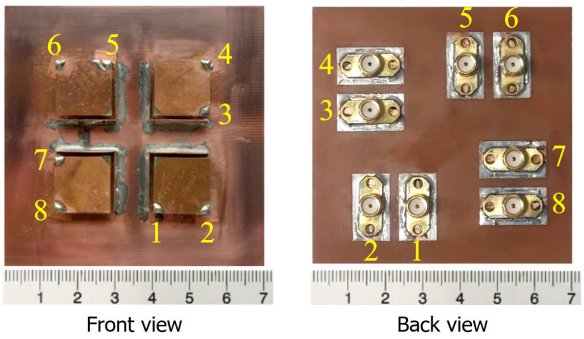

FIGURE 21. Fabricated 2 × 2 DPP antenna array.

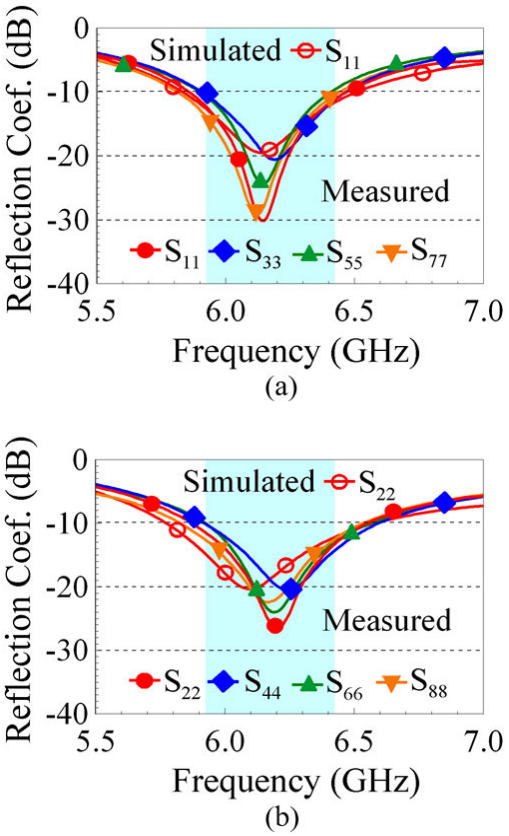

FIGURE 22. Measured reflection coefficients of the fabricated DPP antenna array. (a) Ports 1, 3, 5, and 7. (b) Ports 2, 4, 6, and 8.

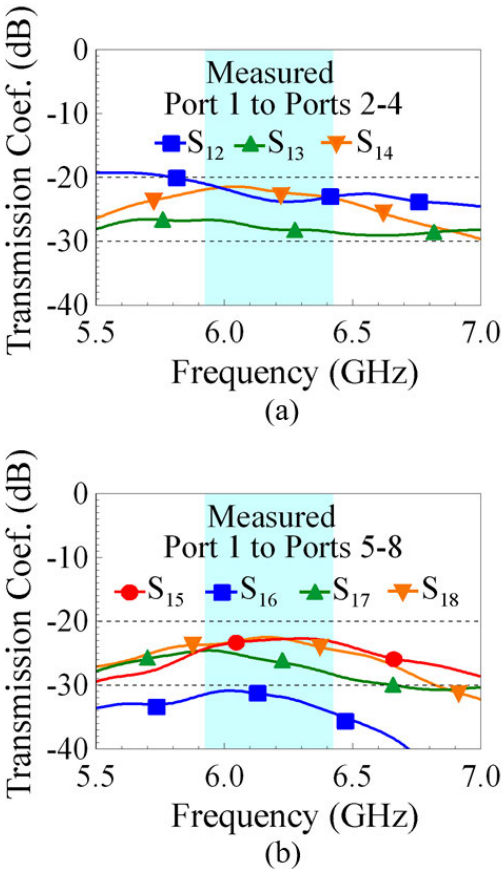

FIGURE 23. Measured transmission coefficients of Port 1 to Ports 2-8 in the fabricated DPP antenna array. (a) The S_{12}, S_{13}, and S_{14}. (b) The S_{15}, S_{16}, S_{17}, and S_{18}.

agree with the simulated results in Figs. 3 and 4 and are less than −20 dB in 5.925-6.425 GHz.

Fig. 25 shows the fabricated DPP antenna array tested in the far-field anechoic chamber to study the antenna radiation characteristics. The antenna array is mounted on a two-axis positioner/rotator and is rotated in both the azimuthal and roll directions so as to obtain its total radiated power and three-dimensional radiation patterns. That is, the Great Circle Test method [30] is applied to obtain the measured antenna efficiency of the fabricated DPP antenna array.

Fig. 26(a) shows the measured antenna efficiency of Ports 1, 3, 5, and 7, which have symmetric locations in the antenna array. Those of Ports 2, 4, 6, and 8, which are located at symmetric array corners, are presented in Fig. 26(b). The measured antenna efficiency is seen to generally agree with the simulated results and is larger than about 84% in the lower 6 GHz band.

Figs. 27 and 28 illustrate the representative measured ECCs of the fabricated DPP antenna array. The ECC values are evaluated by using the measured three-dimensional (3D) complex far-field electric fields [19], [20], [21], [22], [23], [31]. Those for Port 1 to Ports 2-8 are shown in Fig. 27; and those for Port 2 to Ports 3-8 are shown in Fig. 28. The results indicate that the measured ECC values for any two ports in the antenna array are less than 0.02 over the lower 6 GHz band.

Note that the measured ECC values are not so small as the simulated ones (less than10^{-5}) shown in Figs. 6 and 7. The discrepancy may be related to the measurement limitation to obtain very accurate amplitude and phase of the 3D far-field electric fields. However, the measured ECCs are still much less than 0.1 and comparable to those obtained for the 4-port patch antenna [16] and the 8 planar monopole array [23] for access-point applications. The generated 8 waves of the fabricated compact antenna array can thus be considered to be applicable for MIMO system applications.

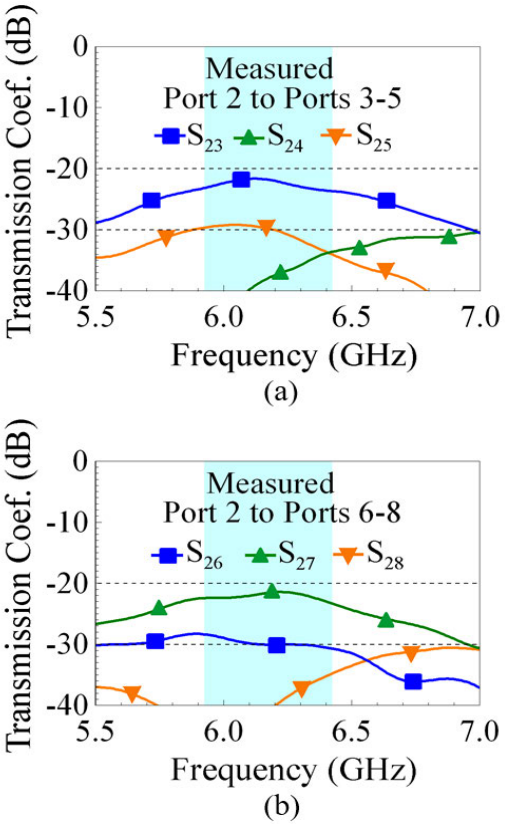

FIGURE 24. Measured transmission coefficients of Port 2 to Ports 3-8 in the fabricated DPP antenna array. (a) The S_{23}, S_{24}, and S_{25}. (b) The S_{26}, S_{27}, and S_{28}.

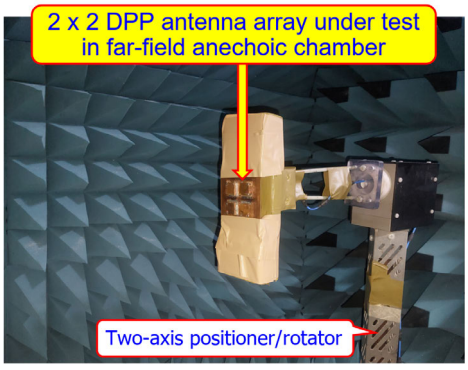

FIGURE 25. Fabricated DPP antenna array tested in the far-field anechoic chamber.

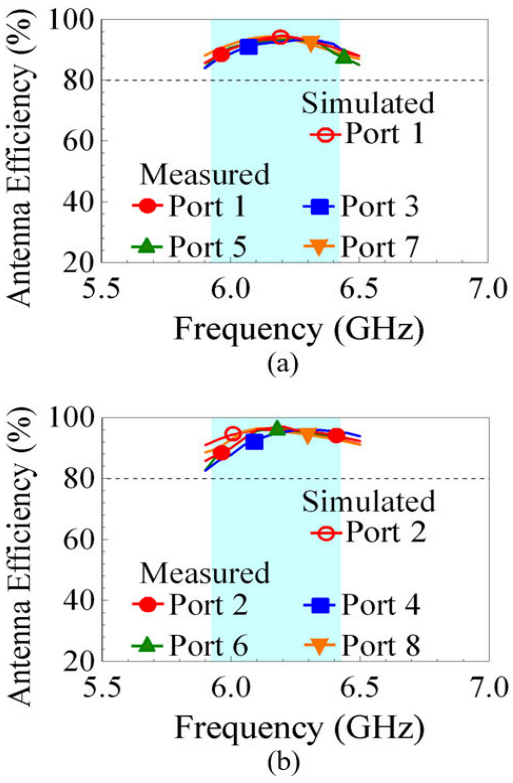

FIGURE 26. Measured antenna efficiency of the fabricated DPP antenna array. (a) Ports 1, 3, 5, and 7. (b) Ports 2, 4, 6, and 8.

Fig. 29 shows the measured and simulated radiation patterns at about the center frequency 6.18 GHz for Ports 1-8 along the resonant direction (either along the $\phi = 45^{o}$ or 135^{o} plane) of their excited resonant modes in the fabricated DPP antenna array. Fig. 30 also shows the measured and simulated antenna gain for Ports 1-8 over the operating band.

The measured radiation patterns and antenna gain generally conform with the simulated results. The antenna gain is about 7.8-9.4 dBi for Ports 1, 3, 5, 7 and about 6.7-8.3 dBi for Ports 2, 4, 6, 8. The antenna gain for Ports 2, 4, 6, and 8 is lower owing to its relatively wider radiation patterns as seen in Fig. 29.

Similar radiation patterns for Ports 1, 3, 5, and 7 plotted in Fig. 29(a) are also seen. Those for Ports 2, 4, 6, and 8 plotted in Fig. 29(b) also show similar patterns. Furthermore, it is seen that the radiation patterns for Ports 1-8 are slightly tilted away from the array center (z-axis or $\theta = 0^{o}$ direction), with those in Fig. 29(b) tilted further away from the array center. This behavior is related to the decoupling metal wall facing asymmetrically to the two ports in each DPP antenna.

VI. THE 8 × 8 MIMO SYSTEM TESTING

To study the MIMO performance of the compact antenna array, we conduct the 8 × 8 MIMO system testing with the fabricated DPP antenna array in an on-campus public indoor space inside the electrical engineering department building at National Sun Yat-sen University (NSYSU). In the study, the 8 × 8 MIMO system testbed [20] shown in Fig. 31 is applied.

As shown in the figure, the fabricated DPP antenna array is used to transmit 8 spatial streams. That is, the DPP antenna array is applied as transmit (Tx) antennas in the WiFi-6E access point. Additionally, an additional one of the proposed DPP antenna array is fabricated to serve as 8 receive (Rx) antennas at the receiver side. That is, a second DPP antenna array is used as Rx antennas for the WiFi-6E user.

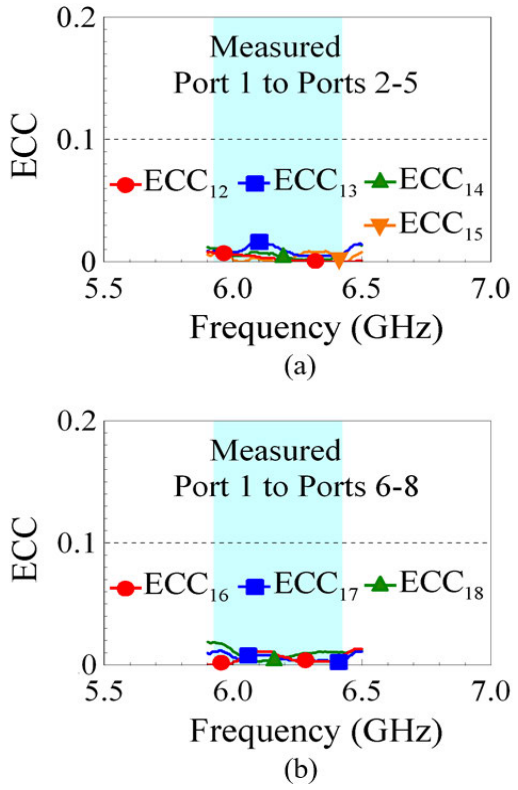

FIGURE 27. Envelope correlation coefficients of Port 1 to Ports 2-8 in the fabricated DPP antenna array. (a) The ECC_{12}, ECC_{13}, ECC_{14}, and ECC_{15}. (b) The ECC_{16}, ECC_{17}, and ECC_{18}.

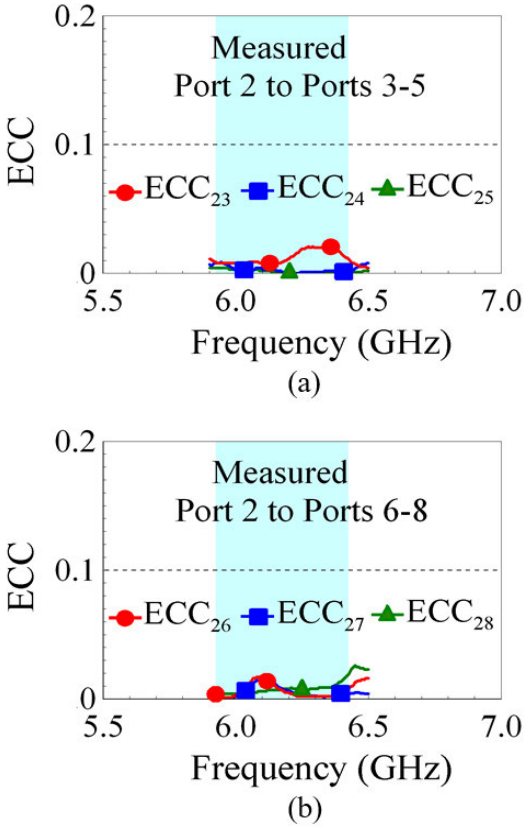

FIGURE 28. Envelope correlation coefficients of Port 2 to Ports 3-8 in the fabricated DPP antenna array. (a) The ECC_{23}, ECC_{24}, and ECC_{25}. (b) The ECC_{26}, ECC_{27}, and ECC_{28}.

Fig. 32 shows the on-campus public indoor space measuring about 19 meters by 6.6 meters for the 8 × 8 MIMO system testing. The conditions of no crowd [Fig. 32(a)] and with crowd [Fig. 32(b)] between the Tx and Rx antennas are tested. The 80 MHz channel (6140-6220 MHz) centered at 6180 MHz (about the center frequency of the lower 6 GHz band) for the 8 × 8 MIMO system operation is studied. The Rx and Tx antennas are placed along the centerline of the indoor space and face to each other. The distance between the Rx and Tx antennas is 7 meters.

Table 2 lists the measured 8 × 8 MIMO system performance. The received signal noise ratios (SNR) of the 8 Rx antennas and their average value are shown. The calculated MIMO capacity is evaluated by assuming the ideally rich multipath condition for the 8 × 8 MIMO system.

On the other hand, the measured MIMO capacity is the practical capacity obtained in the tested public indoor space. The MIMO efficiency is the ratio of the measured MIMO capacity to the calculated MIMO capacity and indicates how well the multipath propagation of the tested public indoor space with respect to the ideally rich multipath condition.

The signal modulation uses 256-QAM (Quadruple Amplitude Modulation) with 8 bits per symbol for the tested 8 × 8 MIMO system. The uncoded bit error rate (BER) is the ratio of the erroneous data received at the receiver to the total transmitted data at the transmitter in the MIMO system. Generally, when the uncoded BER is less than about 0.05 [20], [21], [22], [23], it can be corrected to be zero in the MIMO system with the error correction code. In this case, successful 8 × 8 MIMO system operation with the applied signal modulation (256-QAM here) is achieved.

It is worthy to note that the 8 × 8 MIMO system in this study successfully supports the 256-QAM signal modulation, which is better than the 8 × 8 MIMO system operated in the 7.1 GHz band to support only 64-QAM (6 bits per symbol) in [20] and [23]. This may be partly because the public indoor space in this study with both Tx/Rx indoor scenario is expected to have relatively richer multipath behavior than the Tx outdoor/Rx indoor scenario for the 8 × 8 MIMO system studied in [20] and [23]. With the 256-QAM signal modulation, the achievable data throughput is about 1.33 times that with the 64-QAM only. That is, a faster data transmission speed with a fixed channel bandwidth can be obtained.

Thus, with the 256-QAM signal modulation, the measured throughput (the correct data received at the receiver) in this study for the 80 MHz channel is larger than 3.6 Gbps, which is larger than that (about 3.4 Gbps) obtained for using 100 MHz bandwidth in [20] and [23]. The corresponding spectral efficiency (measured throughput divided by the channel bandwidth 80 MHz) for the 8 × 8 MIMO system is

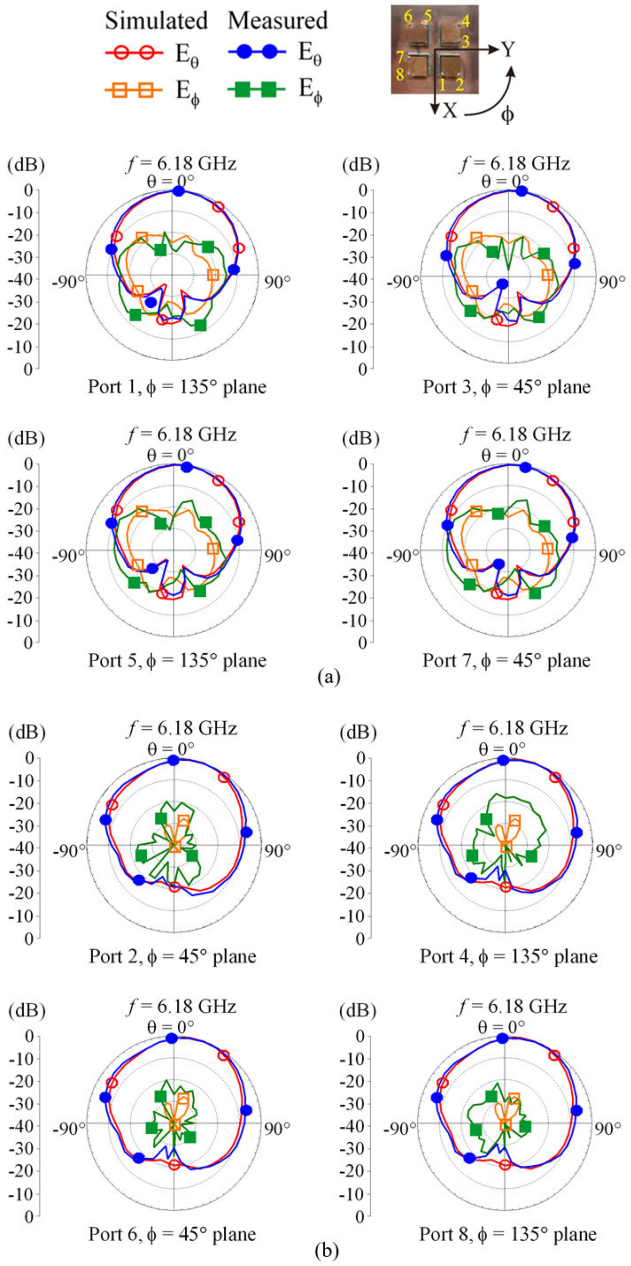

FIGURE 29. Measured and simulated radiation patterns for Ports 1-8 along the resonant direction of their excited resonant modes in the fabricated DPP antenna array. (a) Ports 1, 3, 5, and 7. (b) Ports 2, 4, 6, and 8.

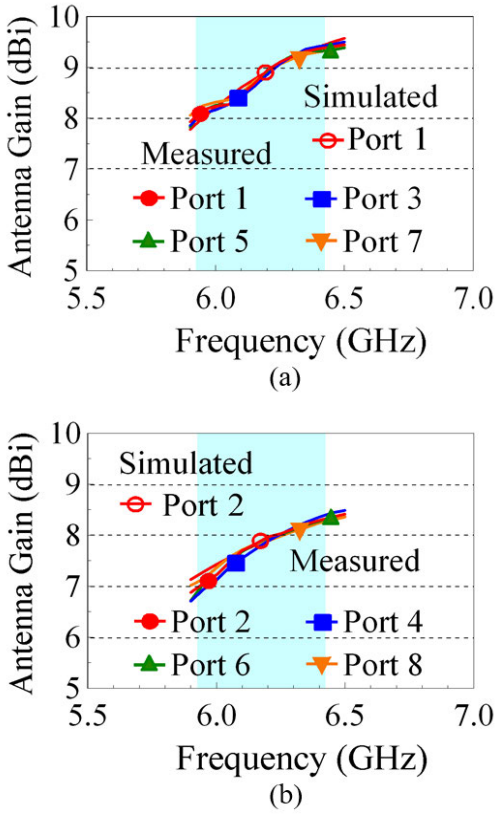

FIGURE 30. Measured and simulated antenna gain of the fabricated DPP antenna array. (a) Ports 1, 3, 5, and 7. (b) Ports 2, 4, 6, and 8.

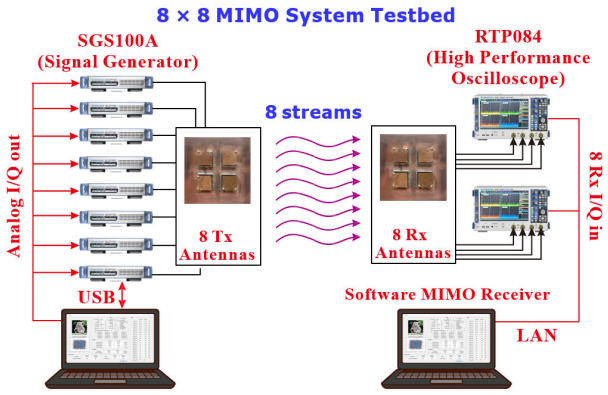

FIGURE 31. The 8 × 8 MIMO system testbed at National Sun Yat-sen University. The fabricated 2 × 2 DPP antenna array in Fig. 21 is used as 8 transmit (Tx) antennas at the transmitter side. An additional 2 × 2 DPP antenna array is also fabricated to be used as 8 receive (Rx) antennas at the receiver side.

larger than 45 bps/Hz, which is larger than about 34 bps/Hz in [20] and [23]. The favorable results obtained here also indicate that the proposed compact DPP antenna array is applicable in the 8 × 8 MIMO system.

It is also interesting to note that when there is crowd gathering in the tested public indoor space (with crowd condition), the 8 × 8 MIMO system can still support the 256-QAM signal modulation and has a spectral efficiency even larger than that of no crowd condition (45.91 vs. 45.54 bps/Hz). This behavior is favorable for practical WiFi-6E applications. The obtained result is probably because the signal's multipath scattering is enhanced owing to the crowd acting as additional scattering objects, instead of blocking the signals, in the tested frequency spectrum (see in the table the MIMO efficiency increased from 76.7% for no crowd condition to 77.8% for with crowd condition).

In addition, note that the measured 8 × 8 MIMO system capacity reaches 53 bps/Hz for either no crowd or with crowd

TABLE 2. Measured 8 × 8 MIMO system performance. The proposed 2 × 2 DPP antenna array is used for both 8 Tx antennas and 8 Rx antennas. The conditions with no crowd and with crowd between the Tx and Rx antennas are tested.

f_0 = 6180 MHz (6140-6220 MHz, 80 MHz channel), 8 × 8 MIMO system, On-campus public indoor space		
Distance of Rx and Tx antennas	7 m	
Signal Modulation	256 QAM	
Testing condition	No crowd condition	With crowd condition
Measured Signal Noise Ratio (dB) of 8 Rx antennas at the receiver side	27.0, 27.4, 29.4, 28.6 27.6, 27.8, 29.3, 27.5 (Ave. SNR ≈ 28.2 dB)	27.6, 27.9, 28.9, 27.5 26.5, 28.0, 28.5, 26.8 (Ave. SNR ≈ 28.1 dB)
Calculated MIMO Capacity (A) (Ideally rich multipath condition)	69.2 bps/Hz	68.1 bps/Hz
Measured MIMO Capacity (B)	53.1 bps/Hz	53.0 bps/Hz
MIMO Efficiency (B/A)	76.7%	77.8%
Uncoded Bit Error Rate	0.030	0.023
Coded Bit Error Rate	0	0
Measured Throughput (T)	3643 Mbps	3672 Mbps
Spectral Efficiency (T/80 MHz)	45.54 bps/Hz	45.91 bps/Hz

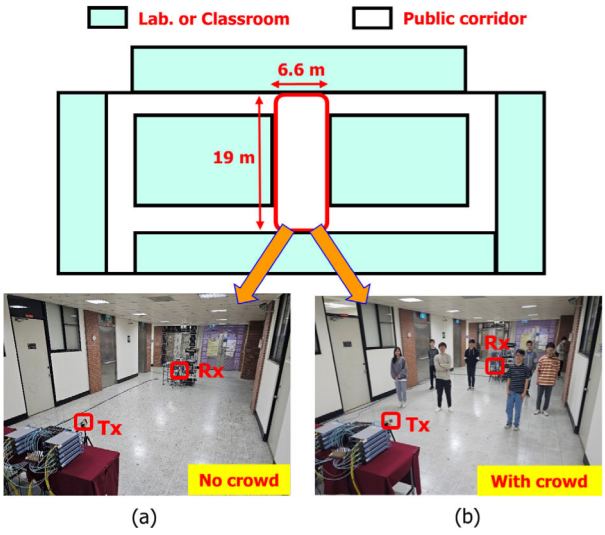

FIGURE 32. The public indoor space inside the electrical engineering department building, NSYSU, for the 8 × 8 MIMO system testing. (a) No crowd condition. (b) With crowd condition.

condition. This implies that, for the maximum 160 MHz channel in the WiFi-6E [2], the 8 × 8 MIMO system capacity based on using the compact DPP antenna array studied here can be about 8.48 Gbps (53 bps/Hz × 160 MHz), reaching 88% of the WiFi-6E's ideal projected system capacity of 9.6 Gbps [3]. The available wide channel of 160 MHz is owing to the 6 GHz band added to the spectrum of previous WiFi generations [2], [32]. This indicates that the proposed compact DPP antenna array is promising for the WiFi-6E application and the ideal projected 8 × 8 MIMO system capacity of 9.6 Gbps is very likely to be feasible, especially in an MIMO environment with much richer multipath propagation than the tested public indoor space in this study.

VII. CONCLUSION

The compact 2 × 2 DPP patch antenna array for the WiFi-6E 8 × 8 MIMO access point application has been proposed. The compact antenna array operates in 5.9-6.5 GHz band and covers the lower 6 GHz band (5.925-6.425 GHz) with a small size of 40 mm × 40 mm. The array size is only about $0.66\lambda^2$ at 5.9 GHz for generating 8 uncorrelated waves. The port isolation of the compact antenna array is also larger than 20 dB over the operating band, which is owing to each one of the 4 DPP antennas therein clad with an L-shape metal wall. The operating principle and design considerations of the compact DPP antenna array have been addressed. Additionally, the fabricated DPP antenna array has been studied and applied in the 8 × 8 MIMO system in an on-campus public indoor space to test its practical MIMO performance. The obtained results show that the proposed compact DPP antenna array is applicable for the WiFi-6E application.

REFERENCES

[1] (Jan. 3, 2020). *Wi-Fi Alliance Brings Wi-Fi 6 Into 6 GHz, Wi-Fi Alliance*. [Online]. Available: https://www.wi-fi.org/news-events/newsroom/wi-fi-alliancer-brings-wi-fi-6-6-ghz

[2] (Jun. 1, 2020). *A Guide to Wi-Fi 6E—Wi-Fi 6 in the 6 GHz Band, LitePoint Whitepaper*. [Online]. Available: https://www.litepoint.com/wp-content/uploads/2020/06/Wi-Fi-6E-Whitepaper-060220-web.pdf
[3] (Jul. 1, 2020). *Next-Generation Wi-Fi: Wi-Fi 7 and Beyond, Intel Corporation*. [Online]. Available: https://www.intel.com/content/dam/www/public/us/en/documents/pdf/wi-fi-7-and-beyond.pdf
[4] (Jan. 3, 2023). *Countries Enabling Wi-Fi in 6 GHz Band, Wi-Fi Alliance*. [Online]. Available: https://www.wi-fi.org/countries-enabling-wi-fi-in-6-ghz-wi-fi-6e
[5] (Aug. 1, 2022). *The 6 GHz IMT Ecosystem: Demand Drives Scale, GSM Association*. [Online]. Available: https://www.gsma.com/spectrum/wp-content/uploads/2022/08/6-GHz-IMT-Ecosystem.pdf
[6] K.-L. Wong, C.-M. Chou, Y.-J. Yang, and K.-Y. Wang, "Multipolarized wideband circular patch antenna for fifth-generation multi-input–multi-output access-point application," *IEEE Antennas Wireless Propag. Lett.*, vol. 18, pp. 2184–2188, 2019.
[7] C.-Y. Chiu, B. K. Lau, and R. Murch, "Bandwidth enhancement technique for broadside tri-modal patch antenna," *IEEE Open J. Antennas Propag.*, vol. 1, pp. 524–533, 2020.
[8] K.-L. Wong, H.-J. Chang, J.-Z. Chen, and K.-Y. Wang, "Three wideband monopolar patch antennas in a Y-Shape structure for 5G multi-input–multi-output access points," *IEEE Antennas Wireless Propag. Lett.*, vol. 19, pp. 393–397, 2020.
[9] C.-Y. Chiu, S. Shen, B. K. Lau, and R. Murch, "The design of a trimodal broadside antenna element for compact massive MIMO arrays: Utilizing the theory of characteristic modes," *IEEE Antennas Propag. Mag.*, vol. 62, no. 6, pp. 46–61, Dec. 2020.
[10] K.-L. Wong and G.-L. Yan, "Wideband three-port equilateral triangular patch antenna generating three uncorrelated waves for 5G MIMO access points," *IEEE Access*, vol. 10, pp. 893–899, 2022.
[11] D. Manteuffel and R. Martens, "Compact multimode multielement antenna for indoor UWB massive MIMO," *IEEE Trans. Antennas Propag.*, vol. 64, no. 7, pp. 2689–2697, Jul. 2016.
[12] W. Su, Q. Zhang, S. Alkaraki, Y. Zhang, X.-Y. Zhang, and Y. Gao, "Radiation energy and mutual coupling evaluation for multimode MIMO antenna based on the theory of characteristic mode," *IEEE Trans. Antennas Propag.*, vol. 67, no. 1, pp. 74–84, Jan. 2019.
[13] K.-L. Wong, J.-Z. Chen, and W.-Y. Li, "Four-port wideband annular-ring patch antenna generating four decoupled waves for 5G multi-input–multi-output access points," *IEEE Trans. Antennas Propag.*, vol. 69, no. 5, pp. 2946–2951, May 2021.
[14] K.-L. Wong, G.-L. Yan, and W.-Y. Li, "Conjoined yet decoupled wideband multiantenna MIMO linear patch array," *IEEE Access*, vol. 10, pp. 46302–46311, 2022.
[15] K.-L. Wong, H.-Y. Jiang, and W.-Y. Li, "Decoupling hybrid metal walls and half-wavelength diagonal open-slots based four-port square patch antenna with high port isolation and low radiation correlation for 2.4/5/6 GHz WiFi-6E 4 × 4 MIMO access points," *IEEE Access*, vol. 10, pp. 81296–81308, 2022.
[16] K.-L. Wong, X.-Q. Ye, and W.-Y. Li, "Wideband four-port single-patch antenna based on the quasi-TM1/2,1/2 mode for 5G MIMO access-point application," *IEEE Access*, vol. 10, pp. 9232–9240, 2022.
[17] N. Peitzmeier, T. Hahn, and D. Manteuffel, "Systematic design of multimode antennas for MIMO applications by leveraging symmetry," *IEEE Trans. Antennas Propag.*, vol. 70, no. 1, pp. 145–155, Jan. 2022.
[18] K.-L. Wong, Z.-W. Tso, and W.-Y. Li, "Very-wide-band six-port single-patch antenna with six uncorrelated waves for MIMO access points," *IEEE Access*, vol. 10, pp. 69555–69567, 2022.
[19] M. S. Sharawi, "Printed multi-band MIMO antenna systems and their performance metrics [wireless corner]," *IEEE Antennas Propag. Mag.*, vol. 55, no. 5, pp. 218–232, Oct. 2013.
[20] K.-L. Wong, H.-C. Kao, and W.-Y. Li, "Wideband low-profile eight-port eight-wave annular-ring patch antenna based on using eight dual-shorted dual-resonant ring sectors for 8 × 8 MIMO mobile devices," *IEEE Access*, vol. 11, pp. 18–32, 2023.
[21] K.-L. Wong, S.-E. Hong, and W.-Y. Li, "Low-profile four-port MIMO antenna module based 16-port closely-spaced 2 × 2 module array for 6G upper mid-band mobile devices," *IEEE Access*, vol. 11, pp. 110796–110808, 2023.
[22] K.-L. Wong, S.-E. Hong, Y.-S. Tseng, and W.-Y. Li, "Low-profile compact 8-port MIMO antenna module and its 1 × 2 array for 6G 16 × 8 device MIMO application," *IEEE Access*, vol. 11, pp. 137011–137024, 2023.
[23] K.-L. Wong, Y.-R. Chen, and W.-Y. Li, "Eight-planar-monopole MIMO circular array generating eight uncorrelated waves for 6G upper mid-band 8 × 8 MIMO access points," *IEEE Access*, vol. 11, pp. 68018–68030, 2023.
[24] Y.-M. Zhang, S. Zhang, J.-L. Li, and G. F. Pedersen, "A transmission-line-based decoupling method for MIMO antenna arrays," *IEEE Trans. Antennas Propag.*, vol. 67, no. 5, pp. 3117–3131, May 2019.
[25] J.-S. Row, S.-H. Yeh, and K.-L. Wong, "Compact dual-polarized microstrip antennas," *Microw. Opt. Technol. Lett.*, vol. 27, no. 4, pp. 284–287, Nov. 2000.
[26] K.-L. Wong, S.-W. Su, and Y.-L. Kuo, "A printed ultra-wideband diversity monopole antenna," *Microw. Opt. Technol. Lett.*, vol. 38, no. 4, pp. 257–259, Aug. 2003.
[27] X. Zhang, D. Zhou, Y. Li, K. Wei, and Z. Zhang, "A simple dual-polarized patch antenna array for Wi-Fi 6/6E application," *IEEE Trans. Antennas Propag.*, vol. 70, no. 11, pp. 11143–11148, Nov. 2022.
[28] (Mar. 1, 2022). *3D High Frequency Electromagnetic Simulation Software, ANSYS HFSS*. [Online]. Available: https://www.ansys.com/products/electronics/ansys-hfss
[29] M. Manteghi and Y. Rahmat-Samii, "Multiport characteristics of a wide-band cavity backed annular patch antenna for multipolarization operations," *IEEE Trans. Antennas Propag.*, vol. 53, no. 1, pp. 466–474, Jan. 2005.
[30] Y. Okano and K. Cho, "Antenna measurement system for mobile terminals," *NTT DoCoMo Tech. J.*, vol. 9, no. 2, pp. 43–50, 2007.
[31] A. Iqbal, A. Altaf, M. Abdullah, M. Alibakhshikenari, E. Limiti, and S. Kim, "Modified U-shaped resonator as decoupling structure in MIMO antenna," *Electronics*, vol. 9, no. 8, p. 1321, Aug. 2020.
[32] K.-L. Wong, H.-J. Chang, C.-Y. Wang, and S.-Y. Wang, "Very-low-profile grounded coplanar waveguide-fed dual-band WLAN slot antenna for on-body antenna application," *IEEE Antennas Wireless Propag. Lett.*, vol. 19, pp. 213–217, 2020.

KIN-LU WONG (Fellow, IEEE) received the B.S. degree in electrical engineering from National Taiwan University, Taipei, Taiwan, in 1981, and the M.S. and Ph.D. degrees in electrical engineering from Texas Tech University, Lubbock, TX, USA, in 1984 and 1986, respectively.

From 1986 to 1987, he was a Visiting Scientist with the Max-Planck-Institute for Plasma Physics, Munich, Germany. Since 1987, he has been with the Electrical Engineering Department, National Sun Yat-sen University (NSYSU), Kaohsiung, Taiwan, where he became a Professor, in 1991. From 1998 to 1999, he was a Visiting Scholar with the ElectroScience Laboratory, The Ohio State University, Columbus, OH, USA. He was elected to be a Sun Yat-sen Chair Professor and a Distinguished Chair Professor with NSYSU, in 2005 and 2017, respectively; a Distinguished Researcher with the National Science and Technology Council of Taiwan, in 2012; and the National Chair Professor and the Lifetime National Chair Professor of the Ministry of Education (MOE), Taiwan, in 2016 and 2023, respectively. He was the Chairperson of the Electrical Engineering Department, from 1994 to 1997; the Vice President for Research Affairs, from 2005 to 2007; and the Senior Vice President with NSYSU, from 2007 to 2012. He is currently the Director of the 6G Communication and Sensing Research Center funded by MOE. He has authored more than 580 refereed journal articles and 300 conference papers and has personally supervised 57 graduated Ph.D. students. He holds over 300 patents, including 106 U.S. patents. He is the author of *Design of Nonplanar Microstrip Antennas and Transmission Lines* (Wiley, 1999), *Compact and Broadband Microstrip Antennas* (Wiley, 2002), and *Planar Antennas for Wireless Communications* (Wiley, 2003). His published articles have been cited over 36,400 times with an H-index of 89 in Google Scholar.

Dr. Wong served as an IEEE AP-S AdCom Member, an IEEE TRANSACTIONS ON ANTENNAS AND PROPAGATION Paper Awards Committee Member, and an AP-Society Field Awards Committee Member. He received the Outstanding Research Award (three times) from the Taiwan National Science

Council, in 1995, 2000, and 2002. He also received the Outstanding Electrical Engineering Professor Award from the Institute of Electrical Engineers of Taiwan, in 2003, and the Outstanding Engineering Professor Award from the Institute of Engineers of Taiwan, in 2004. In 2008, the research achievements on handheld device antennas of the NSYSU Antenna Laboratory led by Dr. Wong was selected to be the top 50 scientific achievements of the Taiwan Ministry of Science and Technology in the past 50 years, from 1959 to 2009. He was a recipient of the 2010 Outstanding Research Award of the Pan Wen Yuan Foundation and was selected as the top 100 Honor of Taiwan by Global Views Monthly, in 2010, for his contribution to mobile antenna research. He was also a recipient of the Academic Award from the Taiwan Ministry of Education, in 2012. He and his graduate students received the Best Paper Award (APMC Prize) from the 2008 APMC; and the Best Student Paper Award/Young Scientist Award from the 2007 ISAP, the 2008 APMC, the 2009 ISAP, the 2010 ISAP, the 2012 ISAP, and the 2016 ISAP. His graduate students also won the First Prize in the 2007 and 2009 Taiwan National Mobile Handset Antenna Design Competition. He received the Best Associate Editor for IEEE TRANSACTIONS ON ANTENNAS AND PROPAGATION, in 2015 and 2016. He was also a PE7 Panel Member of the European Research Council Advanced Grant Panel, in 2015, 2017, and 2019; and the Chief Consultant of the Institute of Antenna Engineers of Taiwan. He also served as the Chair for the Judge Panel of the National Communication Antenna Design Competition organized by the Taiwan Ministry of Economics, from 2014 to 2024. He served as the General Chair for the 2012 APMC, the 2014 ISAP, and the 2016 APCAP held at Kaohsiung, Taiwan; and the Honorary General Chair for the 2023 APMC held at Taipei, Taiwan. He was elected as a Thomson Reuters Highly Cited Researcher, in 2014 and 2015, and an Elsevier Most Cited Researcher, in 2015. In 2022, he was selected by Research.com to be ranked #99 in Full World Ranking and #1 in Full Taiwan Ranking in the 2022 Edition of Ranking of Top 1000 Scientists in the field of electronics and electrical engineering. He served as a Track Editor/an Associate Editor for IEEE TRANSACTIONS ON ANTENNAS AND PROPAGATION.

TZU-CHUN WEI (Student Member, IEEE) received the B.S. degree in electrical engineering from Sun Yat-sen University, Guangzhou, China, in 2021. He is currently pursuing the M.S. degree with National Sun Yat-Sen University, Kaohsiung, Taiwan. His research interests include mobile MIMO antennas for 5G/6G mobile device applications and their higher-order MIMO system performance evaluation.

YU-SHEN TSENG (Student Member, IEEE) received the B.S. degree in electrical engineering from Yuan Ze University, Zhongli, Taiwan, in 2022. He is currently pursuing the M.S. degree with National Sun Yat-sen University, Kaohsiung, Taiwan. His research interests include high-density MIMO antennas for 5G/6G mobile device applications and their higher-order MIMO system performance evaluation.

WEI-YU LI (Member, IEEE) was born in Taipei, Taiwan, in 1981. He received the B.S. degree in electrical engineering from Feng Chia University, Taichung, Taiwan, in 2004, and the M.S. and Ph.D. degrees in electrical engineering from National Sun Yat-sen University (NSYSU), Kaohsiung, Taiwan, in 2006 and 2009, respectively.

After graduating from NSYSU, in 2009, he was with the Information and Communication Research Laboratories (ICL), Industrial Technology Research Institute (ITRI), Hsinchu, Taiwan, participating in and leading advanced research for the development of emerging wireless antenna technologies. From April 2012 to October 2012, he was an Exchange Guest Researcher with the National Institute of Information and Communications Technology (NICT), Tokyo, Japan. He is currently a Technology Manager with ITRI. He has authored and coauthored 36 refereed journal articles and 40 conference papers. He holds over 70 patents, including U.S., Taiwan, China, and EU patents. His published articles have been cited over 1,800 times with an H-index of 24 in Google Scholar.

Dr. Li served as an International Steering Committee Member for ISAP, from 2019 to 2022, and an AdCom Member for the Institute of Antenna Engineers of Taiwan, from 2014 to 2015 and from 2018 to 2023. He also served as a member for the Judge Panel of the National Terminal Antenna Design Competition organized by the Taiwan Ministry of Economics, from 2014 to 2024. He received the Young Scientist Award in the 2007 ISAP and the Best Paper Award (APMC Prize), in 2008. He has been a principal investigator or a co-principal investigator of many research projects at ITRI and has received numerous recognitions, including the First Prize of the Outstanding Research Award of ITRI, in 2010; the Solar Industrial Award (SIA) of Europe, in 2011; the Outstanding Innovation Award of ITRI, in 2013; the Second Prize of the Outstanding Research Award of ITRI, in 2014; the 2015 Research and Development 100 Award Finalist of the U.S.; the Outstanding Innovation Award of ITRI, in 2017; the First Prize of the Outstanding Industrialization Award of ITRI, in 2017; the Second Prize of the Outstanding Industrialization Award of ITRI, in 2020; and the Third Prize of the Outstanding Industrialization Award of ITRI, in 2021. He also received the Outstanding Lecturer Award of ITRI, in 2013; the International Paper Award of ICL of ITRI, in 2020; and the Annual Paper Award of ITRI, in 2023. He also served as the Chair for IEEE AP-S Tainan Chapter, from 2021 to 2022.